Profile of the induced 5*d* magnetic moments in Ce/Fe and La/Fe multilayers probed by x-ray magnetic-resonant scattering

L. Sève, N. Jaouen, J. M. Tonnerre, D. Raoux, and F. Bartolomé
Laboratoire de Cristallographie, CNRS/Université J. Fourier, Boîte Postale 166, 38042 Grenoble Cedex 9, France

M. Arend and W. Felsch
1. Physikalisches Institut, Universität Gottingen, Bunsenstrasse 9, 37073 Gottingen, Germany

A. Rogalev, J. Goulon, and C. Gautier
European Synchrotron Radiation Facility, Boîte Postale 220, 38043 Grenoble Cedex, France

J. F. Bérar
Laboratoire de Cristallographie, CNRS/Université J. Fourier, Boîte Postale 166, 38042 Grenoble Cedex 9, France
(Received 26 April 1999)

The element and electronic shell selectivity of x-ray resonant magnetic scattering (XRMS) has been used to investigate the profile of the spin polarization of the 5*d* electronic states of Ce and La across the rare-earth layers in Ce/Fe and La/Fe multilayers. The magnetic contributions to the diffracted intensities have been measured at low angles, at the L_2 edge of the rare earth. In agreement with previous results from x-ray magnetic circular dichroism (XMCD) experiments, the La 5*d* polarization is found to be localized right at the interfaces with the Fe layers, as it is expected from a direct hybridization with the Fe 3*d* states. In the case of Ce/Fe multilayers where Ce is in an α-like electronic state with a complex behavior of the 5*d* magnetic polarization, the XRMS results obtained for two samples with 10 and 22 Å thick Ce layers indicate that the Ce 5*d* polarization decreases slowly from the interfaces towards the center of the layers. This is in agreement with previous XMCD results. However, at least for the two samples which have been investigated, XRMS also suggests that the Ce 5*d* polarization oscillates across the Ce layer with a period equal to the (111) interplanar distance in α fcc Ce. Though compatible with the XMCD findings, this oscillating behavior cannot be derived from its dependence on the Ce layer thickness because of the decrease of the magnetic polarization which prevents us from observing changes in the sign of the XMCD amplitude. [S0163-1829(99)04637-8]

I. INTRODUCTION

Dramatic differences in the physical properties of Ce metal are known to occur depending on its electronic and structural state. The 4*f* electron states being at the border between localization and itinerancy, both aspects can be found in the γ localized and α itinerant phases of elemental Ce, as well as in its compounds with transition metals, depending on the degree of mixing of the 4*f* and conduction electron states. The denser α phase of Ce metal is nonmagnetic. However, in compounds with *d*-band transition metals like $CeFe_2$ or $CeCo_5$ where Ce adopts an α-phase-like electronic structure, its ground state may be magnetically ordered provided that the concentration of the magnetic transition metal is large enough. In that case, the magnetic moments carried by the itinerant 4*f* states are assumed to be induced by their hybridization with the 3*d* states of the transition metal.[1] The situation is far more complex in the case of Ce/Fe multilayers with thin Ce layers.[2] For a thickness lower than about 25 Å Ce adopts the electronic structure of the α phase, as it has been demonstrated by x-ray absorption spectroscopy (XAS) measurements performed at the $L_{2,3}$[3] and $M_{4,5}$[4] edges of Ce. In both cases, the spectra exhibit the two features split by 10 eV which are the signatures of the $4f^0$ and $4f^1$ electronic states found in the α itinerant phase. Beyond that critical thickness, the amplitude of the $4f^0$ feature decreases due to the growth of a γ-like phase in the center of the Ce layers. The existence of an α-like phase on a considerable length near the interfaces with the Fe layers has been attributed to the compressive strain induced on the Ce atoms by the large mismatch between the Ce and Fe layers.[3]

This α-like phase in Ce/Fe multilayers is structurally and magnetically different from the regular α phase of elemental Ce. X-ray scattering and absorption experiments both suggest that Ce is amorphous up to a critical thickness of 40 Å. It is also magnetically different since it is magnetically polarized at room temperature. This has been demonstrated by x-ray magnetic circular dichroism (XMCD) experiments at the $L_{2,3}$ (Ref. 3) and $M_{4,5}$ (Ref. 4) edges of Ce. They show that both the 5*d* and 4*f* states of Ce are magnetically polarized and carry induced magnetic moments in the range of $0.1\mu_B$ per atom, with an antiparallel orientation with respect to the magnetization in the Fe layer. However, the dependences of the XMCD amplitudes upon the Ce layer thickness are quite different at the *L* and *M* edges. From $M_{4,5}$ edges data, Arend *et al.*[5] have recently shown that the induced magnetism of the 4*f* states of α-like Ce does not extend beyond its immediate interface with the Fe layer; in particular, it is suppressed if Ce is separated from Fe by a 5 Å thick La spacer layer. Thus, the 4*f* magnetic order is linked to the direct overlap between the Ce 4*f* and Fe 3*d* orbitals within

one or two atomic layers at the interface. The $5d$ magnetization of Ce is much more complex, and in some features surprising, since it extends significantly far from the interface. This is clearly demonstrated by the existence of a XMCD signal at the L_2 edge of Ce when a 20 Å thick La spacer layer is inserted between the Ce and Fe ones.[5] Actually, two different magnetic regimes have been observed by XMCD as a function of the Ce thickness in Ce/Fe samples. In regime 1, the mean $5d$ magnetic polarization decreases rapidly from the interface up to a distance of about 10–12 Å while beyond that thickness, in regime 2, it decreases slowly as the inverse of the thickness of the Ce layer. This intriguing behavior suggests that within a few Å from the Fe interface, the Ce $5d$ states are polarized by hybridization with the spin split $3d$ states of Fe, while in regime 2 the magnetic order on the $5d$ states would not result from such a mechanism but rather be an intrinsic property of the ground state of α-like Ce itself in multilayers. The lack of a detailed picture has prompted us to use x-ray resonant magnetic scattering (XRMS) at the L_2 absorption edge of cerium to probe the spatial behavior of the $5d$ polarization in a direct way. We have also investigated a La/Fe multilayer at its La L_2 edge in order to validate the use of the method since, in that case, XMCD results[4,5] provide a simple and reliable model for the $5d$ polarization. A dramatic reduction of the XMCD amplitude is indeed observed at the $L_{2,3}$ edges of La when a 5 Å thick Ce layer is inserted between the La and Fe ones. This indicates that the magnetic $5d$ polarization of La is restricted to the direct interface with the Fe layers.

In the past few years, XRMS has become a useful spectroscopic and structural technique allowing to analyze the magnetic properties of complex materials.[6,7] Since it makes use of the resonant enhancement of the magnetic scattering occurring at an absorption edge, it is nothing but x-ray magnetic dichroism in the scattering mode. Therefore, it yields the same spectroscopic information as XMCD which is the imaginary part of its amplitude, including the possible determination of the spin and orbital components of the magnetic moment by using the sum rules.[8] In particular, it has the same chemical and orbital selectivity as XMCD, allowing one to probe the magnetic properties of a specific electronic shell of a given component in a complex material. That is the reason why XRMS has been recently used as a spectroscopic tool to investigate the magnetization of $3d$ transition-metal atoms in multilayers. These experiments have been mostly performed in the soft x-ray range,[9–11] because of the strong XMCD amplitude at the $L_{2,3}$ edges of $3d$ transition metals. However, being a scattering technique, XRMS also provides structural information on the magnetic ordering. Therefore, we use it here to determine the profile of the induced $5d$ magnetic polarization throughout the rare-earth layer by measuring the magnetic contributions to the multilayer diffraction peaks at the $L_{2,3}$ edge of the rare earth. The experiments have been performed at low angles on the diffraction peaks provided by the chemical modulation of the multilayers. Unfortunately, no diffraction peaks related to the rare-earth phases were observed at large angles, the stacking of the layers being not coherent enough throughout the samples. Nevertheless, a structural information with an atomic resolution may still be recovered from scattering at low angles if a sufficiently large number of peaks is measured. A $[\mathrm{La}(40\,\text{Å})/\mathrm{Fe}(30\,\text{Å})]\times 30$ multilayer and two Ce/Fe multilayers with different Ce thickness but with the same 30 Å thick Fe one, have been investigated. The $[\mathrm{Ce}(10\,\text{Å})/\mathrm{Fe}(30\,\text{Å})]\times 50$ sample has been chosen because the 10 Å thickness of the Ce layers corresponds to the limit of the first regime of magnetic polarization and the $[\mathrm{Ce}(22\,\text{Å})/\mathrm{Fe}(30\,\text{Å})]\times 50$ one because its 22 Å Ce thickness corresponds to the second regime.

II. THE XRMS METHOD

A. The XRMS scattering factor

At the L_2 edge of a rare-earth, XRMS results from the electric dipole transition from the $2p^{1/2}$ atomic core level towards the unoccupied $5d^{3/2}$ states which carry the magnetic moment. As for XMCD, the magnetic sensitivity arises from the exchange splitting of the unoccupied $5d$ states induced by their magnetic polarization and from the spin polarization of the photoelectron which is related to the spin-orbit coupling in the $2p$ core level. We have chosen to work at the L_2 edge because the XMCD amplitude is the same as at the L_3 one but is purely of a dipolar origin. This is not the case at the L_3 edges of rare-earth atoms where XMCD amplitudes exhibit a noticeable quadrupolar contribution,[12] the angular dependence of which is different from that of the dipolar part. Following Hannon *et al.*,[13] the resonant x-ray atomic scattering factor of a magnetic atom may be written as

$$f(k,E) = -(\hat{\mathbf{e}}_f^* \cdot \hat{\mathbf{e}}_i)[f_0 + f'(E) - if''(E)] - i(\hat{\mathbf{e}}_f^* \times \hat{\mathbf{e}}_i)\cdot\hat{\mathbf{z}}[m'(E) - im''(E)]. \quad (1)$$

E is the photon energy and $\mathbf{k}$ is the scattering vector. $\hat{e}_i$ and $\hat{e}_f$ are the polarization vectors of the electric field for the incident and scattered x-ray beams, which are complex ones for a circular polarization. $\hat{\mathbf{z}}$ is the unit vector along the direction of the magnetization. The first term in Eq. (1) is the regular charge scattering factor by the electrons of the atom, which includes the resonant contribution associated to the absorption edge. The second one is the resonant magnetic scattering factor. Its energy-dependent complex amplitude is related to the matrix elements of the dipolar transition.[13] Its angular dependence is different from the charge one since it depends on the projection of the cross product of the polarization vectors along the direction of the magnetization, so that the polarization undergoes a rotation in the XRMS scattering. Actually, another contribution does exist, the imaginary part of which corresponds to the linear magnetic dichroism. However, its amplitude is far lower, especially at low scattering angles in the longitudinal geometry which we use,[7] so that it can be neglected in our case. $f_0(k)$ is the atomic form factor which is tabulated.[14] $f'(E)$ and $f''(E)$ are the real and imaginary parts of the resonant anomalous complex scattering factor. Tabulated values[15] have been used for Fe. However, they cannot be used for the rare-earth atoms since they do not include the resonant features occurring at the L_2 edge. We have thus determined $f''(E)$ values for Ce and La from the measurements of the x-ray-absorption coefficient of the samples performed at room temperature using the dispersive XAS station at Lure.[3,5] The $f'(E)$ values have been

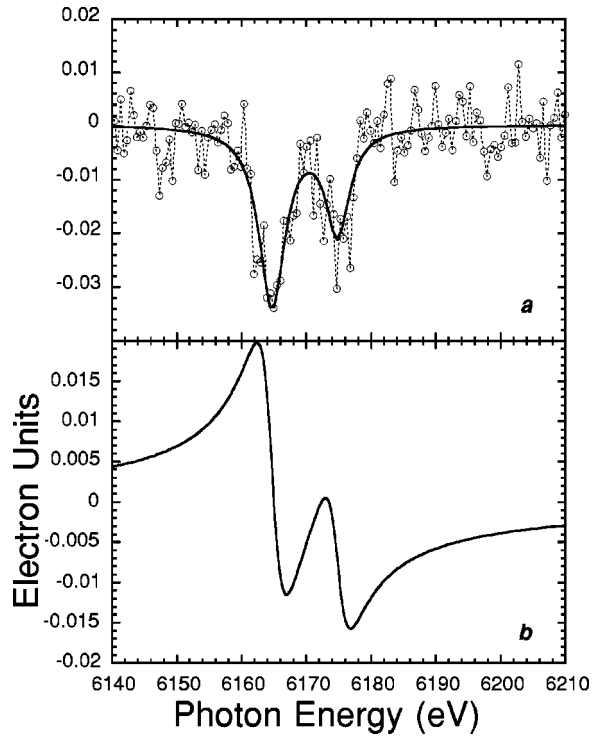

FIG. 1. Values in electron units of the imaginary (a) and real (b) parts of the Ce resonant magnetic factor at the L_2 edge. Open circles in (a) are the experimental values calculated from XMCD data measured for the Ce_{10}/Fe_{30} multilayer, the smoothed curve being a Lorentzian fit. The real part shown in (b) has been calculated as the Kramers-Kronig transform of the Lorentzian fit.

evaluated from the $f''(E)$ data set by using the Kramers-Kronig relation. The $m''(E)$ imaginary parts of the magnetic scattering factors for Ce and La have been evaluated from the corresponding XMCD measurements,[3,5] by scaling to the $f''(E)$ values. The $m'(E)$ real parts have been calculated from the $m''(E)$ ones using the Kramers-Kronig relation. As an example, Fig. 1(a) shows the $m''(E)$ values measured at the Ce L_2 edge for the Ce_{10}/Fe_{30} sample, while Fig. 1(b) displays the $m'(E)$ ones obtained using the smoothed values of $m''(E)$ also shown in Fig. 1(a). We point out that the magnitudes of the $m'(E)$ and $m''(E)$ values are weak, in the range of a few 10^{-2} electron units. We thus expect the XRMS contributions to the diffracted intensities to be weak.

In order to enhance them, we chose the longitudinal scattering geometry shown in Fig. 2 with an elliptical polarization. It allows the amplitudes of the charge and magnetic scattering to interfere, so that the magnetic contribution to the diffracted intensity occurs to first order in a crossed term. The magnetization lies in the vertical scattering plane and in the plane of the layers, at an angle θ with the incident and scattered x-ray beams, 2θ being the scattering angle. In such a geometry, the scattering factor of the magnetic atom the edge of which is investigated, is given for the two polarization states of the scattered beam by, respectively,

$$f_\sigma(k,E)+\epsilon m_\sigma(k,E)=-\frac{f(k,E)+\epsilon K\cos(\theta)m(E)}{(1+K^2)^{1/2}}, \quad (2)$$

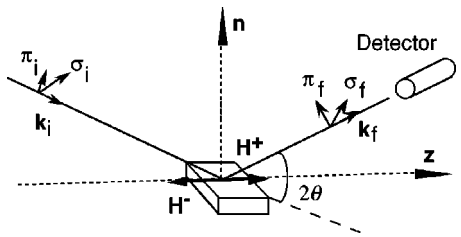

FIG. 2. Schematic picture of the longitudinal geometry used in the XRMS experiment with the magnetic field **H** lying simultaneously in the plane of the sample and in the scattering plane. $\mathbf{k}_i(\mathbf{k}_f)$ is the wave vector of the incident (scattered) x-ray beam; σ_i (σ_f) and π_i (π_f) are the unit vectors of the polarization states of the electric field for the incident (scattered) beam, perpendicular and parallel to the scattering plane, respectively.

$$f_\pi(k,E)+\epsilon m_\pi(k,E)=-\frac{f(k,E)K\cos(2\theta)-\epsilon\cos(\theta)m(E)}{(1+K^2)^{1/2}} \quad (3)$$

with $\epsilon=\pm 1$ depending on the orientation of the magnetization $\hat{\mathbf{z}}$ with respect to $\hat{\mathbf{e}}_i\times\hat{\mathbf{e}}_f$. K is the ratio of the amplitudes of the ϵ (vertical) to π (horizontal) components of the elliptical electric field, so that the rate of circular polarization of the x-ray beam is $\tau=2K/(1+K^2)$. As shown in Eqs. (2) and (3), this geometry maximizes the magnetic scattering at low angles since the magnetic term depends on $\cos(\theta)$ for both polarization states.

B. The calculation of the asymmetry ratio

The magnetic scattering being weak, it is easier to bring out an effect by flipping the magnetization by reversing an applied magnetic field strong enough to align the directions of magnetization of all the Fe layers. I^+ and I^- being the intensities scattered for the two opposite directions of the field, we define R, the asymmetry ratio, as

$$R=\frac{(I^+-I^-)}{(I^++I^-)}. \quad (4)$$

To calculate the diffracted intensities, we used the simple kinematic approximation which proved to be correct even for the first low-angle peak since it allows us to simulate accurately its angular shape as well as the Kiessig fringes due to the sample thickness. In this approximation, the intensity is the sum of the intensities diffracted along both polarization states of the scattered beam, each one including a charge and a magnetic contribution. They are the product of the atomic scattering factors given in Eqs. (2) and (3) by the appropriate structure factors of the multilayer. The structure factors themselves are the products of two contributions, that of a single unit cell the height of which is the period of the multilayer, and that resulting from the stacking of all the periods throughout the multilayer. However, the values of the asymmetry ratio do not depend on the last contribution which is eliminated in the ratio. We then define $F(k,E)$ and $M(k,E)$ as the charge and magnetic atomic complex structure factors of the unit cell as a function of the coordinates z of the atomic planes along the direction of growth of the multilayer and of σ, the Fe and Ce or La atomic densities in the planes of the layers:

$$F(k,E)=F_r-iF_i=\sum_{\text{unit cell}}(f_0+f'-if'')\sigma e^{ikz}, \quad (5)$$

$$M(k,E)=M_r-iM_i=\sum_{\text{mag.at.}}(m'-im'')\sigma e^{ikz}. \quad (6)$$

A straightforward but tedious calculation[7] yields the expression of the asymmetry ratio

$$R=\frac{-2\tau\cos^3*(\theta)[F_rM_r-F_iM_i]}{\cos^2(\theta)|M^2|+\left(1-\frac{K\tau\sin^2(2\theta)}{2}\left|F^2\right|\right)}. \quad (7)$$

As expected, the R values increase almost linearly with τ. Their dependence on $\cos^3*(\theta)$, which is due to the geometry and to the use of an elliptic polarization, maximizes their amplitude at low angles.

In the calculation of $F(k,E)$, the summation has to be performed over all the atomic planes within one period of the multilayer, while the calculation of M only runs over those of the planes which contain the magnetic Ce (or La) atoms whose edge is investigated. In the case of the Ce/Fe samples, a difficulty arises from the fact that the Ce layers are amorphous, so that there are no well-defined Ce atomic planes. We cannot use directly expressions (5) and (6). In order to get the profile of magnetization at an atomic scale, we divide the amorphous Ce layer into slices with a height d equal to the regular interatomic distance in the crystalline fcc phase of α Ce. The charge and magnetic structure factors are then obtained by changing in Eqs. (5) and (6) the planar atomic density σ for $(2\rho/k)\sin(kd/2)$, with ρ being the three-dimensional atomic density given by $\rho=\sigma/d$. At the low-k values at which our experiments have been performed, the differences between the values of the structure factors calculated for a crystalline or an amorphous model are weak. Actually, in the case of the Ce_{10}/Fe_{30} sample the intensities of the four diffraction peaks could be simulated by using the formalism of the crystalline structure factor but by reducing by about 10% the planar densities σ. We nevertheless used the formalism of the scattering by an amorphous Ce layer.

The structural parameters required to calculate $F(k,E)$ and $M(k,E)$ have been determined from a structural study mentioned in Sec. III. In the calculation of M, we assumed that all the rare-earth atoms carry the same magnetic moment within an atomic La plane or an elemental Ce slice, and thus have the same values of atomic magnetic scattering factor $m'(E)$-im$''(E)$, which may however vary from plane to plane, or slice to slice. Indeed, the mean value of the m'' imaginary parts averaged over the period of the multilayer, is given by the XMCD amplitude. Therefore, the true parameters are the ratios of the m'' factors to their mean value, which are called atomic polarization in the following. Their number is equal to n-1, n being the number of atomic planes, or of amorphous slices containing rare-earth atoms. It is large when the rare-earth sublayer is thick. In order to reduce it, we can assume that the magnetic ordering is symmetric with respect to the center of the rare-earth sublayer. Actually, the pertinent parameters in the calculation of M are the values of the magnetic polarization integrated over an atomic plane or an elemental slice. They are related to the values of the atomic polarization, whose determination is the goal, by the partial density of magnetic atoms in the slice. To get rid of a specific model for the magnetic profile of the $5d$ polarization of the rare-earth atoms, we developed a procedure to simultaneously refine the energy dependencies of all the measured asymmetry ratios and directly determine all the parameters. To do so, we used a least-squares routine which is an extension of the DPU package written by Wolfers.[16] This is easy to do in the frame of the kinematic approximation which we use.

C. Experimental procedure

The XRMS experiments have been performed at the ESRF ID12A beam line which is dedicated to polarization-dependent x-ray-absorption spectroscopy.[17] Left-handed circular polarized x rays were generated with the Helios 2 helical undulator.[18] The fixed exit double-crystal monochromator was equipped with a pair of two Si (111) crystals. Due to the very low emittance of the ring, the energy resolution was close to the theoretical limit, 0.6 eV at the Ce L_2 edge (6164 eV). The rate τ of circular polarization of the monochromatic beam was around 84% at that energy and 82% at the La L_2 edge. As it is shown in Secs. IV and V, the XRMS contributions to the diffracted intensities are pretty weak, in the range of a few 10^{-3}. Therefore, in order to get meaningful values of the asymmetry ratios, an extremely high accuracy is required in the measurement of the diffracted intensities, as well as an excellent stability in the position, the size, and the orientation of the beam impinging on the sample. Actually, the position of the beam, which has a cross section of 100 μm (horizontal) by 10 μm (vertical), was found to be stable within 5 μm and its direction within a few μrad. The highly efficient detection system implemented on the beam line allowed us to collect spectra with the very high signal-to-noise ratio required in our experiments. The detector is a silicon photodiode associated with a digital lock-in exploiting the modulation of the x-ray beam at 68 Hz.[19] At each point of measurement, this allows to get rid of the unwanted dark current of the photodiode and of slow drifts of the electronics. As a consequence, a noise figure below a few 10^{-5} was obtained for the diffracted intensities. A two circles diffractometer with horizontal axes has been installed for the experiment. The angular resolution was set at 0.005 degrees by the receiving slits. A coil wound around a U-shaped iron yoke was mounted on the sample stage. It delivered in the plane of the sample a magnetic field of 600 G strong enough to saturate the magnetization in the Fe layers and to ferromagnetically couple them.

III. SAMPLE PREPARATION AND STRUCTURAL CHARACTERISTICS

We recall here briefly the procedure of preparation of the samples which is described in more detail elsewhere.[2,3] The multilayers were grown by computer-controlled ion-beam sputtering in a ultrahigh vacuum chamber (base pressure $p<5\times10^{-10}$ mbar). Highly pure sputtering gas Ar ($6N$) and target metals La, Ce ($3N$) and Fe ($4N8$) were used. Partial pressures of reactive gases (O_2, N_2, H_2O) were kept below 10^{-10} mbar during the deposition process. The samples have

been grown on Si (100) wafers coated with a 40 Å thick Cr buffer layer, with growth rates around 1.0 Å/s for La and Ce, and 0.5 Å/s for Fe. A 50 Å thick Fe capping layer provided protection against oxidation. The deposition of the multilayers has been performed at about 90 K to minimize diffusion. As a consequence, due to the well-defined layered structure of the sample with sharp composition profiles, up to 11 diffraction peaks could be registered at low angles in the case of the La/Fe multilayer.

The period of the multilayers, the respective thickness of their Fe and La or Ce sublayers, their atomic densities, as well as the roughness at their interfaces have been determined from the fit of the x-ray reflectivity at low angles using the optical theory of x-ray reflectivity.[20] Their values are given for the La/Fe and Ce/Fe samples in Tables I in Sec. IV, and II and IV in Sec. V, respectively. Indeed, the contrast between the contributions of Fe and Ce (or La) is rather low, the larger atomic volume of the rare earth compensating to some extent its larger atomic number. In order to better decorrelate the structural parameters related to the rare-earth layers from those of the Fe ones, we used x-ray anomalous scattering to change their respective contributions to the low-angle diffraction pattern. The experiments have been performed at several photon energies around the L_2 edge of the rare earth and the K edge of Fe by using the diffractometer installed on D2AM, the French CRG beam line at ESRF.[21] The changes in the f' values by about 6 electrons at both edges are moderate. Nevertheless, significant variations in the intensities of the diffraction peaks were observed as it is illustrated in Fig. 3 which shows the reflectivity patterns measured for the Ce_{10}/Fe_{30} sample at the Ce L_2 and Fe K edges, as well as at an intermediate energy, together with their simulations for the values of the parameters given in Table II. The simulations fit rather well the experimental data beyond the first diffraction peak, the agreement being poorer at very low angles. For the three samples, the determinations of the periods and of the layer thickness given in Tables I, II, and IV are close to their nominal values. In all cases, the interfacial roughness are rather weak, with Gaussian standard deviations lower than one interatomic distance. Nevertheless in the case of the Ce_{10}/Fe_{30} sample, the full widths of both interfaces extend over the whole of the 10 Å thick Ce layer. A slight asymmetry between the two interfaces is also observed for the Ce/Fe samples, in agreement with a previous structural investigation.[2]

The atomic structures of the Fe and La layers have been previously determined by conventional x-ray diffraction at large angles.[2,22] In both the Ce/Fe and La/Fe samples, the 30 Å thick Fe layers grow along the (110) direction in the bcc structure, the interplanar distance being close to the regular one in bulk Fe (2.027 Å). In the case of the Ce/Fe samples, the diffraction patterns show however a weak contribution of (211) domains. In the La/Fe sample, the La layers grow along the (111) orientation in the β fcc phase, with an interplanar distance close to that in bulk β La (3.026 Å). The values of the Fe and La atomic densities determined from the simulation of the x-ray anomalous reflectivity and reported in Table I are found to be that of bulk bcc Fe and fcc La, in agreement with the diffraction results. In the case of the Ce/Fe multilayers (Tables II and IV), the refined values of the Fe atomic density are also that of bulk bcc Fe. The

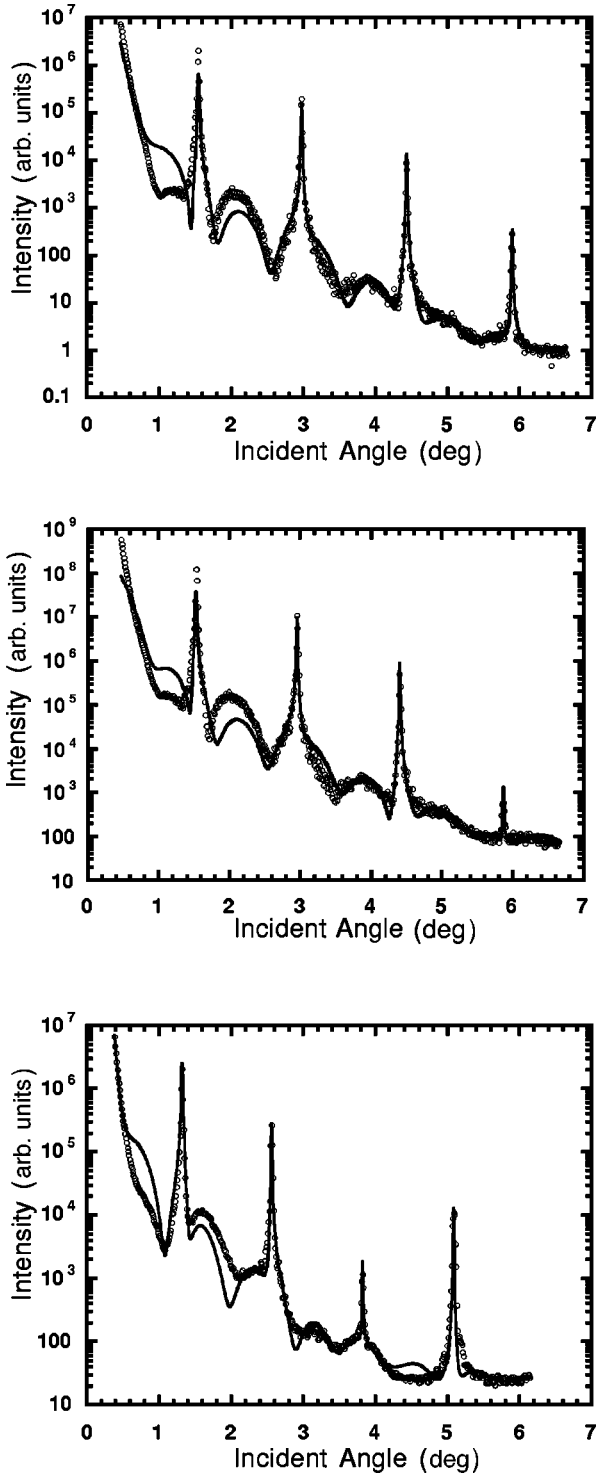

FIG. 3. Low-angle diffraction patterns of the Ce_{10}/Fe_{30} sample measured at the Ce L_2 edge (6164 eV), at an intermediate energy (6200 eV) and at the Fe K one (7112 eV), from top to bottom. Open circles show the experimental results and full lines the best simulations of the reflectivity obtained for the values of parameters given in Table II.

atomic structure of the Ce layers is however not well known since previous works[2,22] suggest that Ce is amorphous for a Ce thickness below 40 Å. Beyond that thickness, Ce layers grow in a regular γ fcc phase with a (111) orientation. Indeed the diffraction patterns of both Ce/Fe samples do not exhibit any diffraction peak related to a crystalline Ce phase. For the

Ce_{22}/Fe_{30} sample, the simulation of the x-ray anomalous reflectivity indicates that the value of the Ce density is that of the crystalline α phase ($\rho = 0.0351$ at/Å^{-3}) and is significantly larger than that of the γ phase ($\rho = 0.0291$ at/Å^{-3}). This supports the assumption of an α-like state for Ce in multilayers with Ce thickness lower than 40 Å. In the case of the Ce_{10}/Fe_{30} sample, the simulation of the reflectivity at low angles appears to be far less sensitive to the actual values of the atomic densities. Good fits of the anomalous reflectivity for the Bragg diffraction peaks could be obtained using regular values of the densities of bcc Fe and α fcc Ce, especially at the *K* edge of iron as it is shown in Fig. 3. At the Ce L_2 edge, the agreement is however poorer at the first diffraction peak. Values of the Ce densities lower by as much as 30% also produced decent simulations. However, the Fe *K* edge data allows to rule out such a possibility. In the following, we will thus assume that the Ce atomic density is that of the crystalline α phase and that the local amorphous structure is similar to that in the (111) planes of α Ce.

IV. PROFILE OF THE LA-5*d* MAGNETIC POLARIZATION IN A LA/FE MULTILAYER

Figure 4 shows the energy dependences of the asymmetry ratios measured at the L_2 edge of La for eight low angle satellites, together with their simulations. The first-order one could not be accurately measured because the diffraction peak is too close to the plateau of total reflection. Their amplitudes are pretty weak, with maximum values in the range of a few 10^{-3}. Nevertheless, rather good-quality data have been obtained up to the ninth order. The spectral shapes exhibit a dispersionlike behavior with a single Lorentzian resonance in agreement with the single Lorentzian feature displayed by XMCD data.[3] They look essentially like the real part of the magnetic atomic scattering factor. This is expected from Eq. (7) since the real part of the structure factor *Fr* is much larger than the imaginary one *Fi*. The strong variation of the amplitudes of the asymmetry ratios with the scattering angle is a direct evidence that the 5*d* magnetic polarization is not constant throughout the La layers. In such a case, both the charge and the magnetic structure factors, *F* and *M*, would have the same *k* dependence, so that the asymmetry ratios would not exhibit any dependence on the order of the diffraction peaks. We point out that the *R* values corresponding to even and odd peaks have opposite signs. This can be qualitatively understood as resulting from a localization of the magnetic polarization at the interfaces with the Fe layers.

In order to derive the profile of the La 5*d* magnetic polarization, the energy-dependent amplitudes of the eight asymmetry ratios have been simulated following the procedure described in Sec. II B and using the structural parameters given in Table I. We point out that the numbers of atomic planes in the Fe and La sublayers are not integer ones. In order that the 75.6 Å period of the multilayer does correspond to an integer number of 31 atomic planes, the Fe (110) interplanar distance has been slightly relaxed by 2.4% in comparison with its bulk value, while keeping the atomic density. The La (111) interplanar distance has been kept at its regular value in the β fcc phase, so that the La sublayer thickness does correspond to 13.6 planes. The values of the roughness derived from the simulation of the x-ray reflectivity, whose standard deviations are given in Table I, indicate that the interfaces between Fe and La sublayers extend roughly over two atomic planes. The resulting profile of the La concentration throughout a La layer is shown in the upper

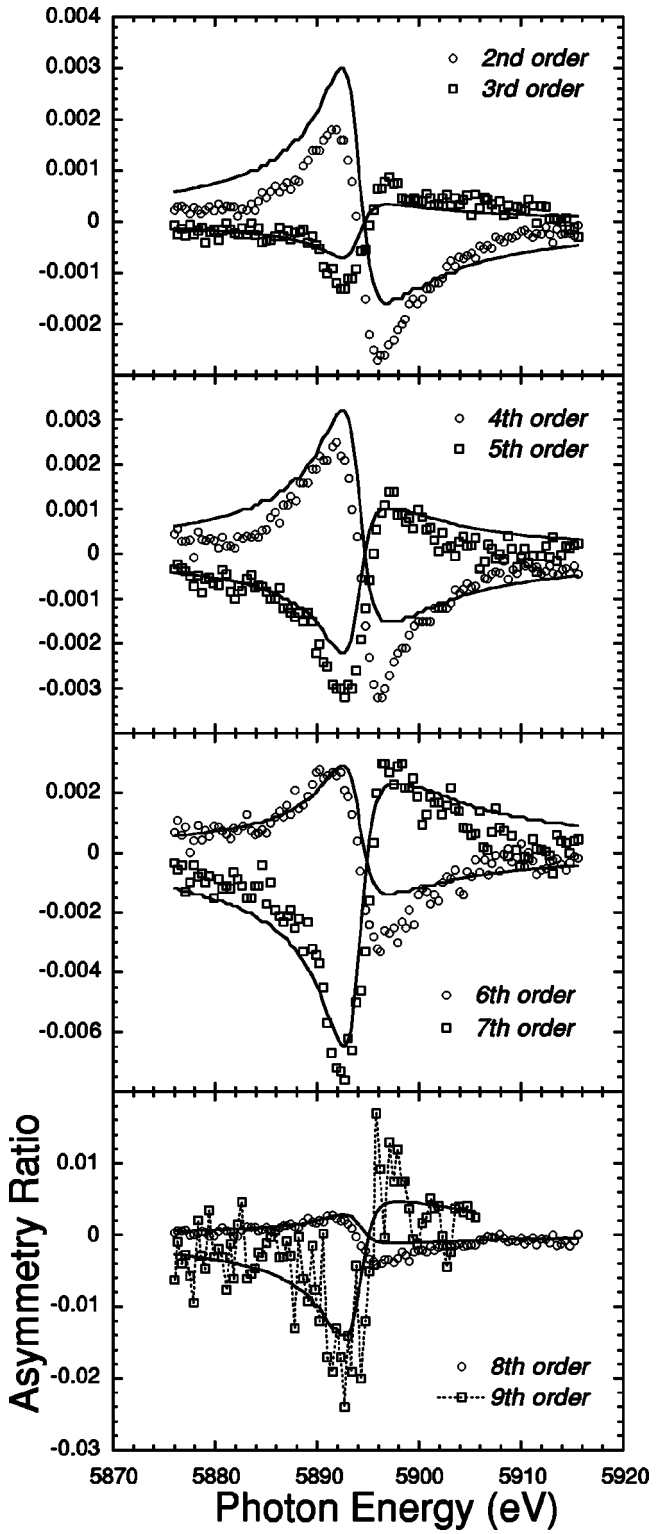

FIG. 4. Energy dependences of the asymmetry ratios at the La L_2 edge for eight low-angle diffraction peaks of the La/Fe multilayer. Open circles and squares show experimental values and full lines the simulations obtained using the profile of magnetic polarization shown in the lower part of Fig. 5.

TABLE I. Structural parameters for the La_{40}/Fe_{30} multilayer. The period, the thickness of the La and Fe layers, the interfacial roughness (standard deviation), and the densities are determined from the refinement of the x-ray anomalous reflectivity. The La interplanar distance is the (111) one for β fcc La and the Fe one is relaxed by 2% compared to the regular (110) interplanar distance in bcc Fe as discussed in text.

Period (Å) 75.6±0.01	La	Fe
Layer thickness (Å)	41.2±0.4	34.4±0.4
Roughness (σ in Å)	La/Fe 2.1±0.3	Fe/La 2.2±0.3
Atomic density (10^{-3} Å^{-3})	26.45	84.92
Interplanar distance (Å)	3.026	1.98
Number of atomic planes	13.6±0.15	17.4±0.2

part of Fig. 5. The two interfacial planes are mixed ones containing, respectively, about 45% and 85% of La atoms.

In order to reduce the number of free parameters in the simulation of the asymmetry ratios, we assumed that the magnetic $5d$ polarization of La atoms is restricted to within 3 planes at each interface with Fe layers, as it is strongly suggested by XMCD results.[3,5] We also assumed a magnetic symmetry, which implies that the magnetic profiles are the same at the La/Fe and Fe/La interfaces. We thus are left with only three adjustable parameters which are the values of the magnetic polarization per La atom in the three planes. This number is even reduced to two by using the constraint that the imaginary part of the mean value of the magnetic polarization averaged over the La layer is given by the XMCD intensity. It is thus far lower than the number of parameters that could possibly be determined from the refinement of the energy dependencies of the eight asymmetry ratios. As a consequence, the determination of the magnetic polarization in each of the three La planes at the interfaces with Fe should be unambiguous.

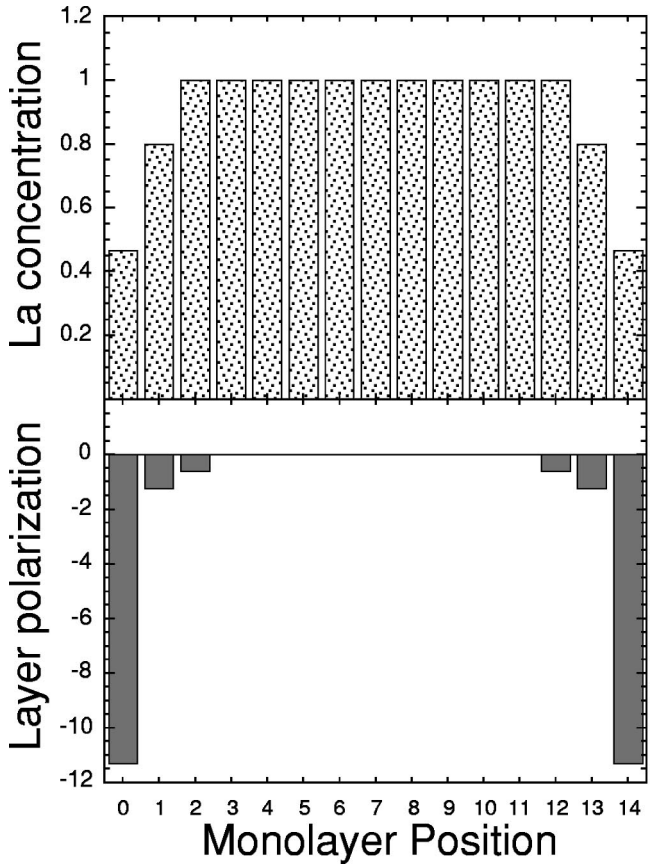

FIG. 5. Profiles across the La sublayer of the La atomic concentration, upper part, and of the $5d$ La magnetic atomic polarization, lower part. The unit of magnetic polarization is the mean polarization averaged throughout the La sublayer which is given by the XMCD amplitude.

Figure 4 shows the simulation of the asymmetry ratios obtained for the magnetic profile displayed in the lower part of Fig. 5. Though not perfect, the agreement between simulations and experimental data displayed is reasonably good, given that only two parameters have been used. As shown in the lower part in Fig. 5, the profile of the $5d$ magnetization carried by a La atom is found to decrease drastically from the interface with Fe towards the center of the La layer. The negative sign of the polarization has been chosen because of the antiferromagnetic ordering of the La layers with respect to the Fe magnetization. The La atomic polarization in the mixed interfacial plane is 11.6 times larger than its mean value averaged over the whole of the La layer; it decreases dramatically to about 1.2 in the next plane containing about 85% La atoms and to 0.6 in the following pure La plane. We point out that such a steep decrease of the polarization is preserved even if the assumption that the polarization is localized only over three planes at the interface is relaxed. These results are qualitatively in agreement with previous XMCD results at the L_2 edge and especially with the strong reduction of its amplitude which is observed when inserting a 5 Å thin Ce spacer layer between La and Fe.[5] From the XMCD measurement for such a multilayer,[3] a value of $0.13\mu_B$ has been determined for the mean magnetic moment averaged over the La layer. We can use it as a scaling factor to evaluate the $5d$ magnetic moments per La atom in each of the three magnetically polarized planes. We get $1.5\mu_B$ in the interfacial plane and $0.16\mu_B$ and $0.08\mu_B$ in the two next ones. The value of the moment in the mixed interfacial plane is pretty large compared to the mean value of $0.13\mu_B$. However, it is in reasonably good agreement with the XMCD measurement of a mean moment of $0.6\mu_B$ per La atom for a La_{10}/Fe_{30} multilayer[3] with a thin La layer containing 3.3 La planes. Finally, we stress that the magnetic profile derived from this XRMS investigation fully supports the model derived by Arend *et al.*[5] from XMCD data, which suggests that the $5d$ states of La at the Fe interfaces are magnetically polarized over one or two atomic layers by direct hybridization with the spin split $3d$ states of Fe.

V. PROFILE OF THE CE-5*d* MAGNETIC POLARIZATION IN CE/FE MULTILAYERS

Figures 6 and 8 display the energy dependences of the four asymmetry ratios which have been measured at the L_2 edge of cerium for the two Ce/Fe multilayers, together with their best simulations. The spectral shapes are quite different from those shown in Fig. 4 for the La/Fe sample. For Ce, two contributions separated by about 10 eV are observed, as it is also the case for the real and imaginary parts of the Ce resonant magnetic atomic factor which are shown in Fig. 1. They

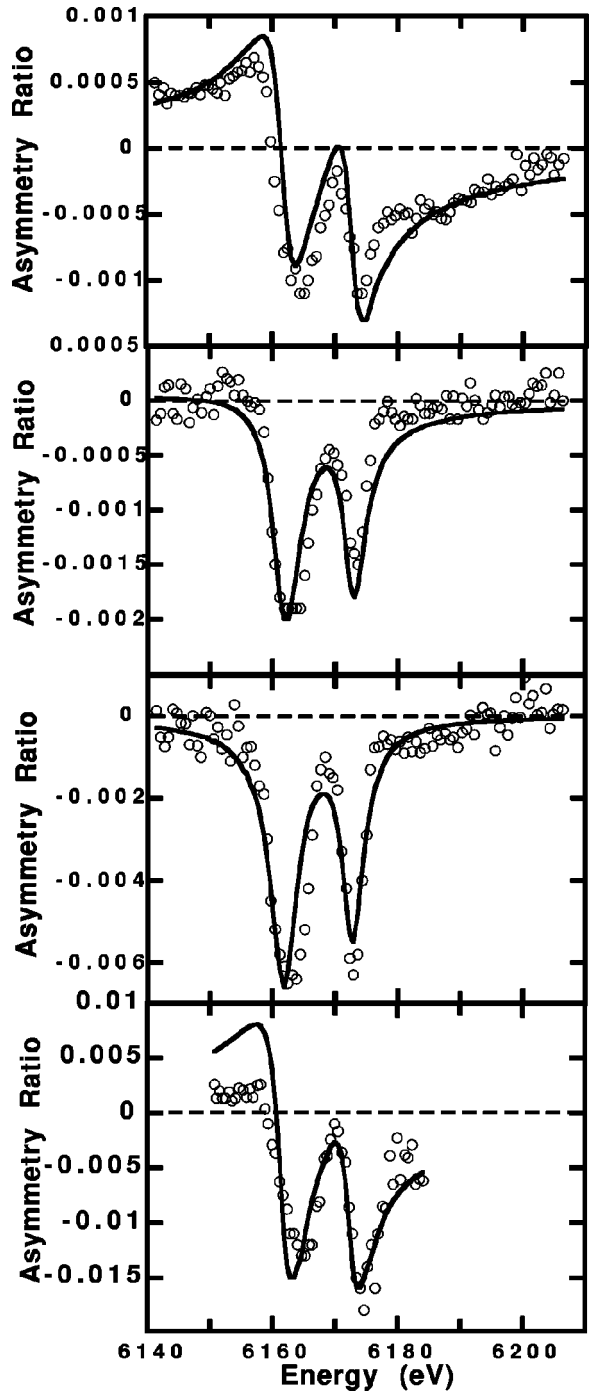

FIG. 6. Energy dependences of the asymmetry ratios at the Ce L_2 edge, for the diffraction pattern of the Ce_{10}/Fe_{30} multilayer. Open circles show the experimental values and full lines the best simulations obtained using the magnetic profile shown in the lower part in Fig. 7.

correspond to the two $4f^1$ and $4f^0$ features observed in the isotropic absorption spectrum of α-like Ce state.[3] This mixture together with the interplay between the real and imaginary parts of the resonant magnetic scattering factor result in a complex spectral dependence. As in the La case, the amplitudes of the *R* values are pretty weak, ranging from a few 10^{-4} to at most 1.5×10^{-2}. They strongly depend on the order of the diffraction peaks. As already explained in Sec. IV, this readily indicates that in both Ce/Fe samples, the 5*d*

TABLE II. Structural parameters for the Ce_{10}/Fe_{30} multilayer. The period, the thickness of the Ce and Fe layers, the interfacial roughness (standard deviation), and the densities are determined from the refinement of the x-ray anomalous reflectivity. The interplanar distances refer to the (111) planes in α fcc Ce and to the (110) in bcc Fe.

Period (Å) 39.25 ± 0.01	Ce	Fe
Layer thickness (Å)	10.10 ± 0.2	29.15 ± 0.2
Roughness (α in Å)	Ce/Fe 2.4 ± 0.2	Fe/Ce 2.8 ± 0.2
Atomic densities (10^{-3} Å^{-3})	35.1	84.92
Interplanar distance (Å)	2.80	2.027
Number of atomic planes or amorphous slices	3.6 ± 0.07	14.4 ± 0.1

Ce polarization is nonconstant across the Ce layers. The simulations of the four asymmetry ratios have been performed following the same refinement procedure as in the La/Fe case. The amorphous structure of the Ce layers is, however, taken into account in the calculations of the Ce charge and magnetic structure factors by dividing the Ce sublayer into slices with a 2.80 Å thickness equal to the (111) interplanar distance of the regular α crystalline fcc phase, as it is explained in Sec. II B.

A. The Ce_{10}/Fe_{30} multilayer

The structural parameters for that sample are given in Table II. Its 10.1 Å Ce thickness corresponds to a noninteger number of 3.6 slices with a 2.80 Å thickness. The total number of Ce slices and of Fe crystalline planes in one period is however an integer one. Two models are possible. In the first one, the Ce layer would be built with two central pure Ce slices and with two interfacial ones with a high Ce concentration of 80%. All attempts to fit the asymmetry ratios on this basis failed. We thus consider the second one only. In that case, the Ce sublayer is divided into five slices: three pure Ce ones inside the layer and two mixed ones at both Fe interfaces which have a low atomic Ce concentration. For such a structural model, the Ce 5*d* magnetic profile is determined by refining the energy dependences of four asymmetry ratios. Due to their different spectral shapes with two lobes, it should be possible to determine at least four independent parameters from this data set. To allow their safe determination, we nevertheless tried first to keep the number of free parameters as low as possible, even at the price of a poorer agreement between data and simulation. Therefore, as in the La/Fe case, we assumed the magnetic structure of the Ce layers to be symmetrical with respect to their centers. By using the constraint relating the mean value of the magnetic polarization to the XMCD amplitude, we then are left with only two adjustable parameters. Unexpectedly, the refinement of the asymmetry ratios yields an oscillatory behavior for the magnetic profile of the 5*d* polarization, with rather large values and with the sign of the magnetization changing from slice to slice. Such an oscillatory solution was not expected from the monotonously decreasing dependence of the amplitude of the L_2 edge XMCD on the Ce thickness. It is, however, found to be stable in the refinement, even when relaxing some of the structural parameters. Actually, the best

TABLE III. Profiles of the values of the Ce partial density and of the 5*d* magnetic polarization across the Ce layer in the Ce_{10}/Fe_{30} sample. The unit of atomic polarization is its mean value averaged over the Ce layer and is given by the XMCD measurement for the sample. The unit of density is that of the crystalline α phase of Ce. Values in the upper lines refer to the structural model taking into account interdiffusion across the Ce layer, while those in parentheses in the lower lines are derived for the simpler but unrealistic model with a lower density and a magnetic symmetry.

Slice	1	2	3	4	5	6
Ce partial	0.15	0.45	0.73	0.89	0.65	0.31
density	(0)	(0.49)	(0.83)	(0.83)	(0.83)	(0.22)
Ce atomic	1.6	−10.6	7.6	−8.8	8.6	−7.2
polarization	(0)	(−8.7)	(5.2)	(−7.1)	(5.2)	(−8.7)

simulation is obtained by relaxing the Ce partial density inside the Ce layer to a value lower by about 20% with respect to its regular value in the α crystalline phase. Conversely, this increases the values of the atomic magnetic polarization by about the same amount and keeps almost constant their products with the Ce partial density, which are the true parameters entering in the refinement. With that anomalous low density, the total number of Ce atoms in the amorphous Ce sublayer would then correspond to that found in a slab of 3.2 (111) atomic planes with the regular density of the α crystalline phase. The agreement is also improved by introducing a slight structural asymmetry at the interfaces, with a lower Ce concentration at the Ce/Fe one than at the Fe/Ce. This is on line with the two different values of the interfacial roughness given in Table II and derived from the simulation of the x-ray reflectivity. For this best simulation, the total number of free parameters is actually four (two values of the magnetic polarization, the Ce density and asymmetry in the Ce concentrations at the interfaces). The values of the atomic magnetic polarization and of the partial Ce density are given for each slice in parentheses in Table III. The units are the mean polarization averaged over a slice and the regular density of the crystalline α phase, respectively. The negative sign of the mean polarization has been chosen because of the net antiferromagnetic ordering of the Ce layers with respect to the Fe magnetization.

Such a too low value of the Ce density has also been derived from the refinement of the anomalous reflectivity at the Ce L_2 edge, as mentioned in Sec. III. It appears as a trick to compensate for features not taken into account in the too simple model used. A more realistic one should be considered at the price of a larger number of free parameters. Indeed, the low Ce partial density suggests the occurrence of a significant interdiffusion in the whole of the thin Ce layer. This is also supported by the values of the standard deviations of the interfacial roughness at the interfaces with Fe sublayers reported in Table II. They result in values of the full widths of the interfaces as large as 5.6 and 6.6 Å so that interdiffusion may occur over the whole of the 10 Å thick Ce layer. We thus have tried a more meaningful model assuming the regular density of the phase, but taking interdiffusion explicitly into account. To get rid of any further structural parameter, we assumed a Gaussian model for interdiffusion and used the values of the roughness given in Table II to

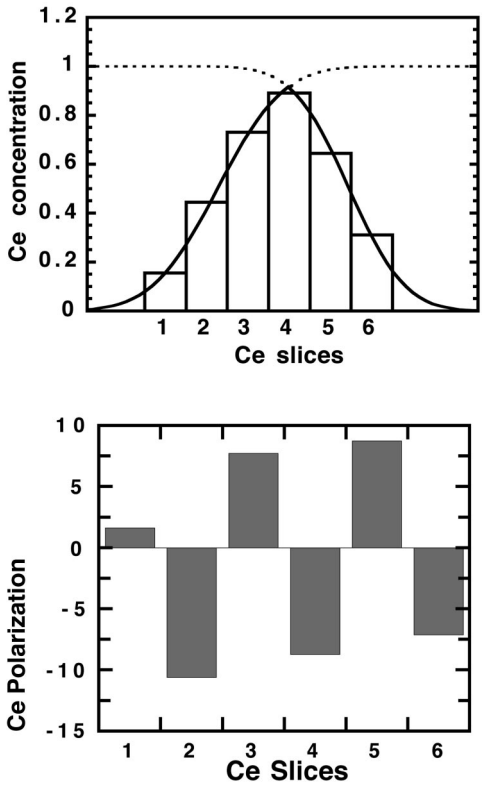

FIG. 7. Profiles across the Ce sublayer in the Ce_{10}/Fe_{30} multilayer, of the Ce atomic concentration, upper part, and of the Ce 5*d* induced magnetic polarization, lower part. The unit of magnetic polarization per Ce atom is the mean polarization averaged throughout the Ce sublayer, which is given by the XMCD amplitude for that sample.

build the profile of the Ce concentration shown in the upper part of Fig. 7. In order to reduce the number of free parameters as much as possible, the Ce layer has been divided into six slices only. The corresponding Ce partial densities are given in Table III. The total number of Ce atoms in the layer corresponds to that found in 3.18 (111) atomic planes in crystalline α Ce. We point out that it is in agreement with that obtained in the simpler but unrealistic model previously discussed. By using the constraint relating the XMCD amplitude to the mean value of the polarization averaged throughout the layer, we are left with five parameters to refine, which are the values of the atomic magnetic polarization in five of the six slices. We did not try to reduce their number by assuming a magnetic symmetry. The refined values of the atomic polarization are given in Table III and the corresponding magnetic profile is shown in the lower part in Fig. 7. Figure 6 compares the measurements of the four spectra to their simulations obtained using this profile. The agreement is rather good. Indeed, the weak polarization in slice 1 is found to be less accurately determined, its weight in the refinement being weak because of the low Ce concentration. Conversely, the values of the polarization in the other slices do not depend much on its actual value, even when reversing its sign.

We point out that we recover an oscillating behavior of the magnetic profile which is almost the same as the one found in the simple but unrealistic model restricting interdiffusion within one interfacial layer at the price of a too low

density. The values of the atomic polarization given in Table III are larger by about 20% than those derived in the first model and shown in parentheses. We point out, however, the good qualitative agreement found in both cases for the values of the polarization integrated over a slice, which are the products of the atomic polarization by the partial Ce density and are the pertinent parameters in the refinement. Interestingly, in both cases, their values are found to be symmetrical in slices 3 and 5 in the inside of the layer, even though no structural or magnetic symmetry has been assumed in the second model. In both cases, the same large magnetic asymmetry is induced in the interfacial slices 2 and 6 by the asymmetry in the concentration profile. We thus stress the stability of the magnetic solution which does not depend on the details of the structural model, despite the fact that a significant interdiffusion occurs in such a sample with a thin Fe layer. We also checked that the oscillating behavior of the magnetic profile is preserved when using a crystalline model for the Ce layers. Actually, provided that the same values of the structural parameters of the multilayer are used, including the Ce density, the values of the magnetic polarization are found to be the same as for the amorphous case, within 10%. Finally, we point out that simple models suggested by the XMCD findings have also been tried as a starting solution in the refinement procedure, but they all failed. Those implying either a constant or a slowly decreasing magnetization throughout the Ce layer give no dependence of the *R* amplitudes on the scattering angle, or a far too weak one. Those with a strong magnetic polarization at the interfaces with Fe, decreasing towards the center of the Ce layer but keeping a negative sign without oscillating, as in the La/Fe case, also failed. Whatever the slope of the decrease, they yield a wrong sign for the *R* value at the third order in the diffraction pattern.

B. The Ce_{22}/Fe_{30} multilayer

As shown in Fig. 8, the amplitudes of the four asymmetry ratios exhibit a strong dependence on the order of diffraction. This indicates a nonconstant magnetization throughout the Ce layer, as in the previous case. The first- and third-order spectra are weaker by almost one order of magnitude. This, together with the decrease of the diffracted intensities with the order of diffraction, makes the third spectrum weak and rather noisy. Due to this, its weight in the refinement of the magnetic structure is weak. We thus try to keep the number of free parameters as low as possible, which implies to assume structural and magnetic symmetries across the Ce layer. Table IV gives the structural parameters needed in the refinement. The numbers of atomic Fe planes or of amorphous Ce slices obtained from the thickness of the Fe and Ce layers using the regular interplanar distances for (110) planes in bcc Fe and (111) ones in α fcc Ce, are not integer. However, their sum corresponds to an integer number of 22 planes as it is required for a periodic stacking. Its 21.85 Å thickness corresponding to a noninteger number of 7.8 slices with a 2.80 Å thickness, two models of the Ce layer are possible, as in the case of the Ce_{10}/Fe_{30} sample. In the first one, the layer is divided into eight slices, the two interfacial ones having a large Ce concentration of 0.9. This model did not allow us to obtain a reasonable fit of the asymmetry ratios. We thus used the structural model with nine slices

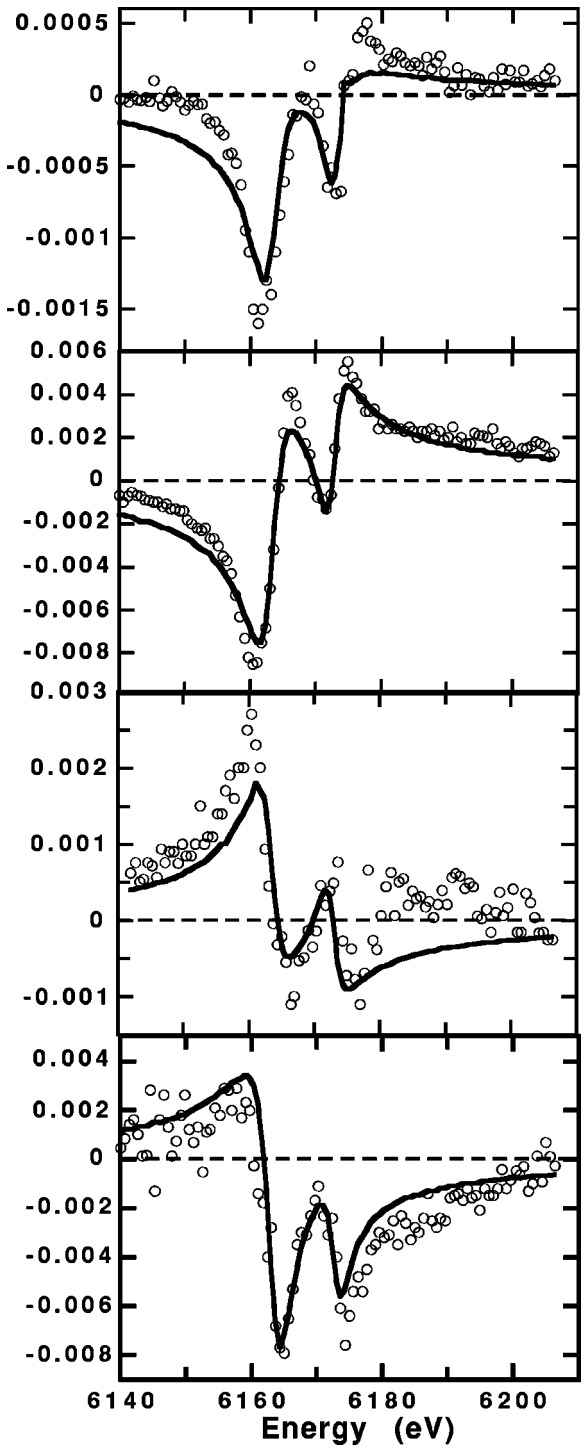

FIG. 8. Energy dependences of the asymmetry ratios at the Ce L_2 edge in the diffraction pattern of the Ce_{22}/Fe_{30} multilayer. Open circles show the experimental values and full lines the best simulations obtained using the magnetic profile shown in the lower part in Fig. 9.

shown in the upper part of Fig. 9. The seven central slices are assumed to be pure Ce ones and the two interfacial ones to be interdiffused with Fe with a Ce concentration of 0.4, as indicated in Table V. This structurally symmetrical model is actually too simple since it does not take into account the interfacial interdiffusion which extends over two slices at each interface, as it is suggested by the values of the standard deviations of the roughness given in Table IV. Nevertheless,

TABLE IV. Structural parameters for the Ce_{22}/Fe_{30} multilayer. The period, the thickness of the Ce and Fe layers, the interfacial roughness (standard deviation), and the densities are determined from the refinement of the x-ray reflectivity. The interplanar distances refer to the (111) planes in α fcc Ce and to the (110) in bcc Fe.

Period (Å) 50.60 ± 0.01	Ce	Fe
Layer thickness (Å)	21.85 ± 0.4	28.75 ± 0.4
Roughness (σ in Å)	Ce/Fe 2.5 ± 0.2	Fe/Ce 2.7 ± 0.2
Atomic densities (10^{-3} Å^{-3})	35.1	84.92
Interplanar distance (Å)	2.80	2.027
Number of atomic planes or amorphous slices	7.8 ± 0.15	14.2 ± 0.2

despite the assumption of a magnetic symmetry with respect to the center of the Ce layer and the use of the constraint that the mean value of the polarization per Ce atom is given by the XMCD measurement, we still are left with four free parameters. Moreover, the fitting of the data proved to be only weakly sensitive to the value of the magnetization in the center of the Ce layer. Thus, we did not try to increase furthermore the number of parameters by taking into account interdiffusion at the interfaces which would introduce additional mixed planes at the interfaces. This should not be a too poor approximation in the case of a 22 Å thick Ce layer, since we have shown that neglecting interdiffusion change the values of the atomic polarization only by about 20% in the far more critical case of a 10 Å thick Ce layer.

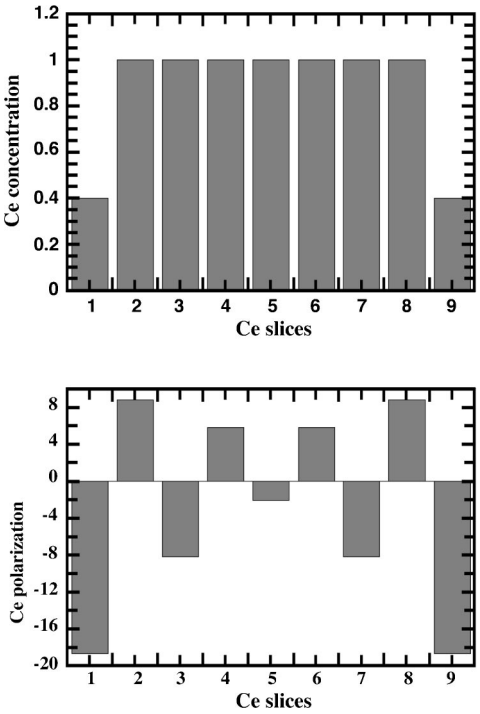

FIG. 9. Profiles across the Ce sublayer in the Ce_{22}/Fe_{30} multilayer of the Ce atomic concentration, upper part, and of the Ce $5d$ induced magnetic polarization, lower part. As in Fig. 7, the unit of magnetic polarization per Ce atom is the mean polarization averaged throughout the Ce sublayer in the Ce_{10}/Fe_{30} multilayer.

The best solution obtained for the magnetic profile is shown in the lower part of Fig. 9, and the corresponding values of the polarization are given in Table V. The unit of polarization is the same as for the Ce_{10}/Fe_{30} sample in order to allow comparison. Figure 8 shows the simulations of the four asymmetry ratios obtained for this best solution. The agreement with experimental data is reasonably good given the low number of parameters in the simulation, even at the third noisy order. Indeed, the factor of merit in the refinement is found to be flat over a range of values of the magnetic polarization in the central slices. In order to allow one to appreciate the accuracy in their determination, error bars corresponding to the extension of that range of possible solutions are given in Table V. The uncertainty in the values of the Ce magnetic polarization decreases strongly from the interfacial slices towards the central ones. In the outer slices, it is lower than 5%, but reaches about 100% in the central one. Nevertheless, the two main characteristics of the polarization profile are preserved for all determinations. First, the profile of polarization is found to oscillate in all cases, with the same period of about 2.80 Å which has been obtained for the Ce_{10}/Fe_{30} sample. Second, the polarization decreases rather slowly from the interfaces towards the center of the layer, except at the interfacial slices interdiffused with Fe, where it is larger than inside the Ce layer.

C. Discussion

The profiles of the $5d$ induced magnetization are found to be qualitatively similar in both samples. Our model, which assumes a ferromagnetic ordering within the Ce slices, gives an antiferromagnetic coupling from slice to slice, with a magnetic period roughly equal to twice the (111) interplanar distance in the α crystalline phase of Ce. As shown in Tables III and V, the decreasing amplitudes of atomic polarization are also comparable in both cases, except in the interfacial slices where they are found to be higher for the Ce_{22}/Fe_{30} sample. We thus have tried to reconstruct them using the same decreasing oscillation for both cases. To do that, the magnetic profiles are assumed to result from the superposition of two damped oscillations decreasing from each interface towards the center of the layer. Their simulation is easier in the case of the Ce_{22}/Fe_{30} sample where a magnetic symmetry has been assumed and where the two oscillations do not interfere much because of the larger thickness. It yields a damped oscillation with a period of 5.9 Å close to twice the (111) interplanar distance, and with amplitudes decreasing roughly as r^{-1}, r being the distance from the interface. In order to allow such a simple analysis, the magnetic profile in the Ce_{10}/Fe_{30} sample has to be made symmetrical with respect to the center of the Ce layer. Interestingly, this symmetrical profile can be simulated using the same damped oscillation than for the Ce_{22}/Fe_{30} sample, provided that a phase shift of about 1.5 Å is introduced to allow to recover the weaker amplitudes of the atomic polarization of the interfacial slices, while keeping the amplitudes of the other slices inside the Ce layer to their values which are close to those in the Ce_{22}/Fe_{30} sample. The origin of this shift, which corresponds to about half an interplanar (111) distance of the crystalline phase, is not clear. It might simply be due to the fact that interdiffusion has not been taken into account in the

TABLE V. Profiles of the values of the Ce partial density and of the 5*d* magnetic polarization across the Ce layer in the Ce_{22}/Fe_{30} sample. To compare with the Ce_{10}/Fe_{30} case, the unit of atomic polarization is the same as in Table III. It is the mean value of the atomic polarization averaged over the Ce layer which is given by the XMCD measurement for the Ce_{10}/Fe_{30} sample. The unit of density is that of the crystalline α phase of Ce. The error bars in the values of the magnetic polarization have been evaluated from the behavior of the factor of merit in the refinement of the asymmetry ratios, as explained in text.

Slice	1	2	3	4	5	6	7	8	9
Ce concentration	0.4	1	1	1	1	1	1	1	0.4
Ce atomic	−18.7	8.8	−8.2	5.8	−2.1	5.8	−8.2	8.8	−18.7
polarization	±0.5	±0.4	±1	±1.5	±1.8	±1.5	±1	±0.4	±0.5

case of the Ce_{22}/Fe_{30} sample. It would extend the thickness over which Ce atoms are distributed and thus shift the magnetic oscillation with respect to the actual positions of the slices used in the refinement procedure. Though such a quantitative comparison should not be pursued too far, it nevertheless suggests that the polarization profiles are actually very similar in the two samples. We like also to point out that they are compatible with the XMCD measurements of net magnetic moments of $0.1\mu_B$ and $0.055\mu_B$ for the Ce_{10}/Fe_{30} and Ce_{22}/Fe_{30} samples respectively, since the mean values of the atomic magnetic polarization averaged over the Ce thickness are 1 and 0.55, the unit being the XMCD amplitude measured for the Ce_{10}/Fe_{30} sample. The absolute values for the magnetic moments can be evaluated by scaling the amplitudes of atomic polarization by $0.1\mu_B$. Rather large values in the range of $1\mu_B$ are obtained. In the case of the Ce_{22}/Fe_{30} sample, they even reach $2\mu_B$ in the mixed interfaces where Fe concentration is large. This has to be compared to the lower values found in Ce_xFe_{1-x} bulk alloys, like for instance the $0.35\mu_B$ moment determined for $CeFe_2$ from XMCD measurements.[23] This reinforces the suggestion that the mechanism responsible for the 5*d* magnetic polarization is not the same in the multilayers and in bulk alloys, the main argument being the observation of an oscillating polarization in the multilayers.

VI. CONCLUSIONS

The XRMS resonant magnetic contributions to the intensity of the Bragg peaks at low angles have been used to determine the profile of the 5*d* induced magnetic polarization of the rare earth in Ce/Fe and La/Fe multilayers. By comparison with XMCD which gives the mean value of the polarization averaged throughout the layer, XRMS does not require the use of several samples with different layer thickness. This is an advantage in the case of a complex nonmonotonous magnetization profile where the comparison of the XMCD amplitudes for various thickness may be inappropriate. This turns out to be the case for the Ce/Fe multilayers investigated in this work. We like also to stress that an atomic resolution has been obtained for the magnetic profiles, even though diffraction data were available only at low angles, up to a scattering vector around 1 $Å^{-1}$. This suggests that such a method could be of a rather broad use to investigate the profiles of magnetization in multilayers and superlattices with periods of a few nanometers, even in cases where the coherence of the stacking is not good enough to provide diffraction peaks at large angles.

The analysis has been performed using the kinematic approximation for diffraction which proved to work in the specific case of these multilayers. Its use being simpler than that of the dynamic theory, it allows one to use refinement procedures to get the magnetization of the rare-earth atoms in each atomic plane, or slice of atomic thickness, without having to assume a specific model. This is an advantage in comparison with the possible use of the resonant magnetic reflectivity outside the diffraction peaks, the analysis of which implies the dynamic optical theory.[10,11]

In the case of the Ce/Fe multilayers, we had to take into account the amorphous structure of the Ce layers, by dividing it into slices having a thickness equal to the regular interplanar distance in α crystalline Ce and by using, for each of these slices, the formalism of the structure factor of an amorphous layer. Actually, since the spectra are obtained at low scattering angles, they depend only weakly on details of the local structure. Very similar magnetic profiles, with changes in the values of the atomic polarization by less than 10%, have also obtained using the formalism of crystalline structure factor. A more serious difficulty originates in the limited number of parameters which can be derived from the simulation of a limited number of asymmetry ratios.

In the simple case of the 5*d* magnetic polarization of La in a La/Fe multilayer where the dependency of the XMCD amplitudes on the thickness of the La layers yields an unambiguous model,[5] the XRMS analysis leads to the same model of magnetic profile, with the 5*d* polarization of La strongly localized in the atomic plane at the interfaces between the La and Fe layers. As discussed in Sec. IV, the agreement is even quantitative. Our result thus fully supports the model of a polarization induced by direct hybridization of the La 5*d* states with the spin split Fe 3*d* ones which has been suggested by Arend *et al.*[5] on the basis of an extensive study of the dependence of XMCD amplitudes on the thickness of the La layer. This example validates the use of the method in the more complex case of the Ce/Fe multilayers.

In the case of the Ce/Fe system, the XRMS results give additional evidence for the very puzzling magnetic behavior of α-like Ce. On one hand, they are in agreement with the main XMCD findings showing that the 5*d* polarization of Ce extends far beyond the interface with Fe,[3,5] and cannot be induced only by direct hybridization with the 3*d* states of Fe. On the other hand, and at least for the two samples which have been investigated, the interpretation of the XRMS spectra provides evidence for an unexpected oscillating behavior of the polarization, with a period roughly equal to twice the (111) interplanar distance of the crystalline phase and with a

slow decrease of its amplitude from the interface towards the inside of the Ce layer. Despite the antiferromagnetic coupling between adjacent slices, a net magnetic moment is nevertheless obtained due to the decrease of the amplitude of the oscillation. Indeed, we recover in both cases the values of the mean atomic magnetic moment which is given by the XMCD amplitude. The decrease of the magnetic polarization, with a weak or null value at about 12 Å from the interface with Fe, is also in agreement with the slow decrease of the XMCD amplitudes with the inverse of the Ce thickness beyond a thickness of 20 Å[3]. However, we stress that such an oscillating profile cannot be inferred from the dependence of the XMCD amplitude on the Ce thickness. The decrease of the amplitudes of the induced magnetic moments from the interface with Fe towards the center of the Ce sublayer prevents one from observing alternate signs in the net moment averaged over the Ce thickness. The observation of an antiferromagnetic coupling between Ce slices, perpendicularly to the growth direction of the multilayer, is rather puzzling. The understanding of its physical origin is not clear at this stage, mainly because of the lack of knowledge of the electronic structure of the amorphous α-like Ce phase in these multilayers which prevent from discriminating between possible mechanisms such as the Ruderman-Kittel-Kasuya-Yosida one or quantum size effects. Further XRMS measurements are needed for a better understanding of the puzzling magnetic properties of the $5d$ electrons in this very special α like Ce state, like, for instance, on samples where a thick La layer is inserted between the Fe and Ce ones without killing the Ce magnetic polarization. We point out that a similar oscillating and decreasing behavior of the magnetic polarization induced in the d band of a nonmagnetic metallic layer has already been observed in the case of a Ru thin layer deposited on a (100) Fe substrate,[24] in an investigation of the spin polarization of the $4d$ band of Ru by Auger $M_{4,5}N_{4,5}N_{4,5}$ spectroscopy. This suggests that such a behavior might not be specific to the Ce case. Finally, we mention that XRMS experiments have been recently performed at the Ce M_4 edge for a Ce_{10}/Fe_{30} sample, in order to get the profile of the $4f$ magnetic polarization. Preliminary results clearly show that, at variance with the $5d$ polarization, the $4f$ one is not oscillating. They suggest that it is almost constant throughout the thin Ce layer. This is in qualitative agreement with XMCD data,[4] which indicate that the $4f$ induced magnetization is strongly localized at the interfaces with Fe and results from direct hybridization with the Fe $3d$ states.

[1] M. S. S. Brooks and B. Johansson, in *Handbook of Magnetic Materials*, edited by K. H. J. Buschow (North-Holland, Amsterdam, 1993), Vol. 7.

[2] F. Klose, M. Steins, T. Kacsich, and W. Felsch, J. Appl. Phys. **74**, 1040 (1993).

[3] F. Klose, O. Schulte, F. Rose, W. Felsch, S. Pizzini, C. Giorgetti, F. Baudelet, E. Dartyge, G. Krill, and A. Fontaine, Phys. Rev. B **50**, 6174 (1994).

[4] M. Finazzi, F. M. F. de Groot, A.-M. Dias, B. Kierren, F. Bertran, Ph. Sainctavit, J.-P. Kappler, O. Schulte, W. Felsch, and G. Krill, Phys. Rev. Lett. **75**, 4654 (1995).

[5] M. Arend, M. Finazzi, O. Schulte, M. Münzenberg, A.-M. Dias, F. Baudelet, C. Giorgetti, E. Dartyge, P. Schaaf, J.-P. Kappler, G. Krill, and W. Felsch, Phys. Rev. B **57**, 2174 (1998).

[6] D. B. Mac Whan, J. Synchrotron Radiat. **1**, 83 (1994), and references therein.

[7] J. M. Tonnerre, in *Magnetism and Synchrotron Radiation*, edited by E. Beaurepaire, B. Carrière, and J. P. Kappler (Les Editions de Physique, Paris, 1997), p. 245, and references therein.

[8] J. M. Tonnerre, L. Sève, D. Raoux, G. Soullié, B. Rodmaq, and P. Wolfers, Phys. Rev. Lett. **75**, 740 (1995).

[9] L. Sève, J. M. Tonnerre, D. Raoux, J. F. Bobo, M. Piecuch, M. De Santis, P. Troussel, J. M. Brot, V. Chakarian, C. C. Kao, and C. T. Chen, J. Magn. Magn. Mater. **148**, 168 (1995); J. M. Tonnerre, L. Sève, D. Raoux, B. Rodmacq, M. De Santis, P. Troussel, J. M. Brot, V. Chakarian, C. C. Kao, E. D. Johnson, and C. T. Chen, Nucl. Instrum. Methods Phys. Res. B **97**, 444 (1995).

[10] M. Sacchi and A. Mirone, Phys. Rev. B **57**, 8408 (1998).

[11] J. M. Tonnerre, L. Sève, A. Barbara-Dechelette, F. Bartolomé, D. Raoux, V. Chakarian, C. C. Kao, H. Fischer, S. Andrieu, and O. Fruchart, J. Appl. Phys. **83**, 6293 (1998).

[12] F. Bartolomé, J. M. Tonnerre, L. Sève, D. Raoux, J. Chaboy, L. M. Garcia, M. Krisch, and C. C. Kao, Phys. Rev. Lett. **79**, 3775 (1997).

[13] J. P. Hannon, G. T. Trammell, M. Blume, and D. Gibbs, Phys. Rev. Lett. **61**, 1245 (1988); *ibid.* **62**, 2644(E) (1989).

[14] D. T. Cromer, Acta Crystallogr. **18**, 17 (1965); D. T. Cromer and J. B. Mann, Acta Crystallogr., Sect. A: Cryst. Phys. Diffr., Theor. Gen. Crystallogr. **A24**, 321 (1968).

[15] S. Sazaki, KEK Report No. 88-14, 1989 (unpublished).

[16] P. Wolfers (private communication).

[17] J. Goulon, A. Rogalev, C. Gauthier, C. Goulon-Ginet, S. Paste, R. Signorato, C. Neumann, L. Varga, and C. Malgrange, J. Synchrotron Radiat. **5**, 232 (1998).

[18] P. Elleaume, J. Synchrotron Radiat. **1**, 19 (1994).

[19] C. Gauthier, G. Goujon, S. Feite, E. Moguiline, L. Braicovich, N. B. Brookes, and J. Goulon, Physica B **208-209**, 232 (1995).

[20] E. E. Fullerton, J. Pearson, C. H. Sowers, S. D. Bader, X. Z. Wu, and S. K. Sinha, Phys. Rev. B **48**, 17 432 (1993).

[21] J. L. Ferrer, J. P. Simon, J. F. Berar, B. Caillot, E. Fanchon, O. Kaikati, S. Arnaud, M. Pirrochi, M. Roth, J. Synchrotron Radiat. **5**, 1346 (1988).

[22] F. Rose, O. Schulte, P. Schaaf, W. Lohstroh, and W. Felsch, Appl. Phys. A: Mater. Sci. Process. **63**, 183 (1996).

[23] C. Giorgetti, S. Pizzini, E. Dartyge, A. Fontaine, F. Baudelet, C. Brouder, P. Bauer, G. Krill, S. Miraglia, D. Fruchart, and J. P. Kappler, Phys. Rev. B **48**, 12 732 (1993).

[24] K. Totland, P. Fuchs, J. C. Gröbli, and M. Landolt, Phys. Rev. Lett. **70**, 2487 (1993).